MIRRORLESS LASING IN OPTICALLY PUMPED RUBIDIUM VAPOR

THESIS

Ryan M. Richards

AFIT-ENP-13-M-41

DEPARTMENT OF THE AIR FORCE
AIR UNIVERSITY

AIR FORCE INSTITUTE OF TECHNOLOGY

Wright-Patterson Air Force Base, Ohio

DISTRIBUTION STATEMENT A. APPROVED FOR PUBLIC RELEASE;
DISTRIBUTION IS UNLIMITED.

The views expressed in this thesis are those of the author and do not reflect the official policy or position of the United States Air Force, Department of Defense, or the U.S. Government.

AFIT-ENP-13-M-41

MIRRORLESS LASING IN OPTICALLY PUMPED RUBIDIUM VAPOR

THESIS

Presented to the Faculty

Department of Physics

Graduate School of Engineering and Management

Air Force Institute of Technology

Air University

Air Education and Training Command

In Partial Fulfillment of the Requirements for the

Degree of Master of Science in Applied Physics

Ryan M. Richards

March 2013

DISTRIBUTION STATEMENT A. APPROVED FOR PUBLIC RELEASE;
DISTRIBUTION IS UNLIMITED.

AFIT-ENP-13-M-41

MIRRORLESS LASING IN OPTICALLY PUMPED RUBIDIUM VAPOR

Ryan M. Richards

Approved:

_____	_____
Glen Perram, Professor, USAF (Chairman)	Date
_____	_____
Brian Tom, Col, USAF (Member)	Date
_____	_____
Anthony Franz, Lt Col, USAF (Member)	Date

Acknowledgments

I would like to thank Professor Glen Perram for his support in conducting this research as well as my family for their encouragement through this process.

Ryan M. Richards

Table of Contents

Page

List of Figures

List of Tables

AFIT-ENP-13-M-41

Abstract

Mirrorless lasing has been successfully demonstrated in a Rubidium heat pipe. Lasing was observed on the $6^2P_{3/2}$-$6^2S_{1/2}$ energy transition at 2.73 μm and on the $6^2P_{1/2}$-$6^2S_{1/2}$ transition at 2.79 μm. The transitions were optically pumped from $5^2S_{1/2}$–$6^2P_{3/2}$ at 420.2 nm and from $5^2S_{1/2}$–$6^2P_{1/2}$ at 421.7 nm, respectively. The $5^2S_{1/2}$–$6^2P_{3/2}$ transition was excited over a 36 GHz band, while the $5^2S_{1/2}$–$6^2P_{1/2}$ transition was excited over a 24 GHz band. Both pump transitions showed a high degree of saturation and only a small fraction (<1%) of the incident pump energy was absorbed. Output energies of up to 5 nJ were obtained at 2.73 μm and of up to 5.4 nJ at 2.79 μm when pumped at pulse energies of ~4 mJ. Both transitions experienced bleaching at this ~4 mJ pump energy, limiting further IR output energy. Increasing rubidium concentration at bleached pump energies showed no increase in laser energy after ~170 $^{\circ}$C, likely due to second order processes. Slope efficiency for both transitions, however, increased linearly with rubidium concentration up to 11 x 10^{-6}. The addition of small amounts of argon, helium, and ethane (5-45 Torr) were found to fully quench lasing action on both transitions.

MIRRORLESS LASING IN OPTICALLY PUMPED RUBIDIUM VAPOR

I. Introduction

The Diode Pumped Alkali Laser (DPAL) was first developed in 2003 (Krupke, 2003) and shown to be a highly efficient three level laser. DPALs have gathered much attention due to the fact they offer the excellent beam quality and cooling efficiency of gas phase lasers, and have shown potential to be effectively scaled to high output powers with good slope efficiency (Bogachev, 2012:95). The typical DPAL operates as a three level laser by optically exciting atomic alkali vapor from its $^2S_{1/2}$ ground state to its lowest $^2P_{3/2}$ state. Collisional relaxation, via some buffer gas (e.g. ethane), then produces a population inversion in the lower $^2P_{1/2}$ state, which subsequently lases back to the ground state. In rubidium this lasing action occurs at 794.5 nm.

Although the majority of DPAL research has analyzed various aspects of the system described above, alternative wavelengths have been observed through various optical excitation methods. The work presented here looks specifically at the $6^2P_{3/2}$-$6^2S_{1/2}$ and the $6^2P_{1/2}$-$6^2S_{1/2}$ transitions at 2.73 μm and 2.79 μm, respectively. The production of a compact laser at these mid-IR wavelengths could prove especially useful as an IR countermeasure to combat the threat of modern IR sensing weapons, such as heat seeking missiles (Titterton, 2006: 635). Mirrorless lasing was first observed at these wavelengths through continuous wave pumping of a heated cell containing rubidium without any buffer gas (Sharma, 1981:209). A further investigation of these transitions is presented here, making use of a pulsed pump source of much larger intensity. The effects of pump

energy, rubidium concentration, and buffer gas on IR signal strength were observed, as well as the IR beam sizes.

II. Background

Chapter Overview

This chapter explores the history of atomic alkali vapor lasers, and in particular, the past analysis conducted on mirrorless lasing in rubidium vapor. The electronic structure of rubidium is shown in Figure 2.1 along with the wavelengths of the pump (420.2 nm and 421.7 nm) and lasing lines (2.73 μm and 2.79 μm) used in this work, as well as the pump and lasing wavelength of the conventional DPAL.

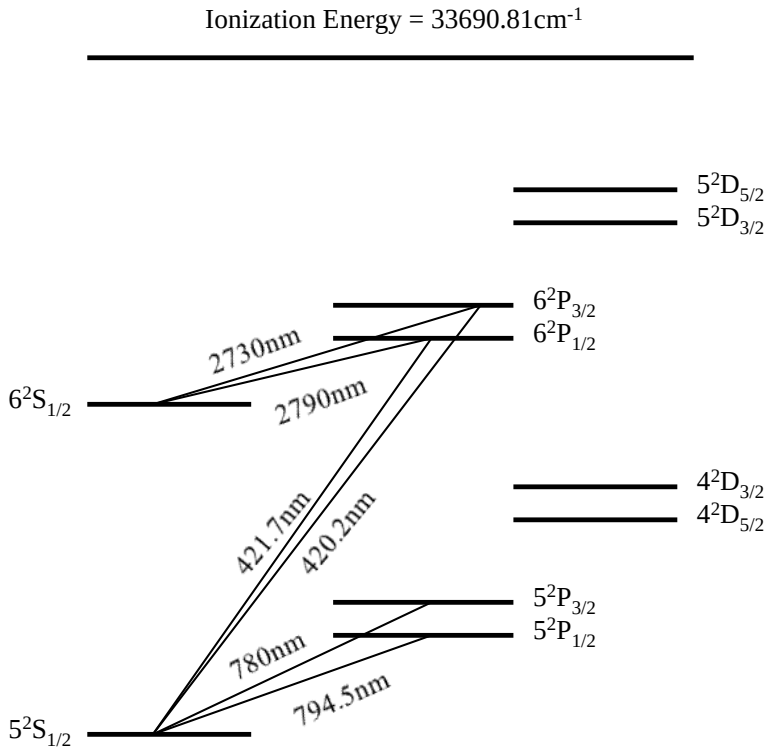

Figure 2.1: Energy level diagram of rubidium with associated pump and laser transition wavelengths.

Listed in Table 2.1 is a collection of laser transitions observed in optically pumped alkali vapors that will be discussed here.

Table 2.1: Observed lasing transitions in K, Rb, and Cs alkali vapors.

Alkali	Pump Wavelength (nm)	Lasing Wavelength (nm)	Reference
K	766.7	770.11	Krupke
	694.3	3140	Sorokin
	694.3	3160	Sorokin
Rb	780.25	794.98	Krupke
	421.7,420.2	1320	Sharma
	421.7,420.2	1370	Sharma
	694.3	2254	Sorokin and Sharma
	694.3	2293	Sorokin and Sharma
	420.2	2730	Sharma
	421.7	2790	Sharma
Cs	852.35	894.59	Krupke
	459.3,765.8	1360	Sorokin and Sharma
	459.3,765.8	1376	Sorokin and Sharma
	459.3,455.5	1469	Sharma
	455.5	2930	Sharma
	459.3,694.3,765.8,740-900,1060	3095	Sorokin and Sharma
	1060	3010	Sorokin
	1060	3489	Sorokin
	1060	3613	Sorokin
	388.8	7180	Rabinowitz

Background

The first suggestion of pumping an atomic alkali vapor in order to achieve stimulated emission came from Schawlow and Townes in 1958 (Schawlow, 1958:1940).

As a means to extend their MASER (**M**icrowave **A**mplification by **S**timulated **E**mission of **R**adiation) work into the optical and infrared, they proposed a system that took advantage of the simple electronic structure of potassium. Their idea was to excite potassium atoms from the $4^2S_{1/2}$ ground state to the $5^2P_{3/2}$ state. These states would subsequently decay to the 5S or 3D states within $2x10^{-7}$ seconds or the ground state more slowly. If, however, the pumping scheme was fast enough, a population inversion could be created in the excited states. For a pump source they proposed using an additional potassium lamp with a spectral filter to allow the transmission of 404.7 nm light, or finding a coincidentally matching spectral line such as that of the 8P level in cesium. They proposed the potassium be held within a sapphire cell with two principle reflecting surfaces placed outside; possibly made of gold or surfaces of alternating high and low dielectric layers. They argued the cell should be long in the path of lasing to gain sufficient energy, while being short in width to decrease the necessary pump powers.

Using this concept, a similar system was devised using cesium vapor in place of the proposed potassium (Rabinowitz, 1962:513). Using an intense helium lamp with a spectral line at 388.8 nm, a population inversion was produced between the $8P_{1/2}$ and $8S_{1/2}$ energy levels, resulting in lasing at 7.18 μm. A 92 cm long by 1 cm inner diameter glass cell was used to heat the cesium to 175 $^{\circ}$C. The resonator cavity was made of a plane and concave reflector coated in silver, and was shown to offer gain of ~1% per cm. The total output power achieved at 7.18 μm was ~25 μW.

As time progressed, sources to pump the necessary transitions in alkali systems became more advanced and allowed for more energy to be coupled into the alkali vapor. By 2003, work was presented that has since served as the benchmark for modern diode pumped alkali lasers (Krupke, 2003). Creating three separate alkali gas systems, Krupke produced lasing at 895 nm in cesium, 795 nm in rubidium, and 770 nm in potassium. Each system operated the same in that the alkali atom's single valence electron was pumped along what is known as the D2 transition, collisionally relaxed to a lower energy state, where it eventually lased back to the ground state along what is known as the D1 transition. A representative example can be seen in rubidium in Figure 2.1 by pumping the D2 transition at 780 nm, and lasing along the D1 transition at 794.5 nm.

Although pumping with diode arrays has proven the most efficient, Krupke initially used a titanium sapphire laser for proof of concept purposes. In order to optimize the overlap between the pump linewidth and the alkali's absorption feature, Krupke found the addition of a moderate amount (100s of Torr) of a rare gas such as helium provided maximum pressure broadening of the absorption linewidth. In order to collisionally relax the alkali atom to the lasing level, a small amount (~100 Torr) of a small molecule like ethane was also added to the system. While optimizing the D2/D1 systems, Krupke also tried to develop a blue laser by using two step pumping to the second excited $^2P_{3/2,1/2}$ states (Krupke, 2006). While he did not succeed in this effort, he did observe infrared emission from the (n+1)P to (n+1)S and (n-1)D states. These IR transitions have also been documented in the past, although not fully investigated.

In 1969, Sorokin used giant pulse (~20 nm linewidth) lasers to pump helium buffered cesium and rubidium gases (Sorokin, 1969:2929). Lasing was observed at 3.095 μm in cesium and at 2.254 μm and 2.293 μm in rubidium. The giant pulse pumping mechanisms consisted of two ruby laser pumped dye lasers for cesium which output 1-2MW/cm^2, and an independent ruby laser for rubidium which required ~500 MW/cm^2 as the rubidium system proved much less efficient. Approximately 1 atm of helium was generally used in each cell, and the alkalis were heated to 340 ˚C in cesium and ~400 ˚C in rubidium. Sorokin next attempted pumping a potassium system with a ruby laser and observed lasing at 3.14 μm and 3.16 μm (Sorokin, 1971:2184).

Building off this work, mirrorless lasing along the $6^2P_{3/2}$-$6^2S_{1/2}$ and the $6^2P_{1/2}$-$6^2S_{1/2}$ transitions in rubidium vapor was produced (Sharma, 1981:209). Using a continuous wave Ar^+ laser to pump a stilbene-3 dye laser, pump wavelengths between 410 nm and 470 nm at powers of 200-300 mW were achieved. Rubidium vapor was produced in a glass bulb that was heated up to 400 ˚C. Emission was observed with a PbS detector cooled to 195 K. Stimulated emission intensity was measured as a function of both incident pump power and rubidium concentration, and shown to be very nonlinear. As the bulb temperature increased from 72–120 ˚C, rubidium concentration varied by a factor of about 16-20, but the infrared fluorescence increased about 200 times. After peaking around 120 ˚C the IR signals decreased almost as quickly over 120–220 ˚C to about 1/5 their peak value. Using a ~1 mm beam, input power was varied from

0-200 mW and IR lasing was analyzed. It was shown that the stimulated emission intensity increased linearly from about 0–40 mW, after which the intensity plateaued and experienced minimal increase with higher input power.

In 2010, Sulham reported on blue and infrared emission along multiple transitions in both cesium and rubidium using two photon absorption methods with a pulsed dye laser pump source (Sulham, 2010:57). The pump was a single 10 Hz red laser with 4 ns pulses with energy up to 100 mJ. The laser was 3.5 mm in diameter and tuned for two photon absorption on the (n) or $(n+1)^2D_{3/2,5/2}$ and (n+2) or $(n+3)^2S_{1/2}$ states in Rb(n=5) and Cs(n=6). The cesium and rubidium vapor were generated in Pyrex cells heated to 175–250 ˚C. Blue emission in Rb was observed along the $6^2P_{3/2} - 5^2S_{1/2}$ and $6^2P_{1/2} - 5^2S_{1/2}$ transitions and infrared emissions were observed along the $7^2S_{1/2} - 6^2P_{3/2}$ transition as well as the $5^2D_{5/2} - 6^2P_{3/2}$ and $5^2D_{3/2} - 6^2P_{1/2}$ transitions. These energy levels are shown in Figure 2.1.

Using the results of Sharma, and optical excitation methods along the blue lines observed by Sulham, the work described here further investigates the $6^2P_{3/2}$-$6^2S_{1/2}$ and the $6^2P_{1/2}$-$6^2S_{1/2}$ transitions at 2.73 μm and 2.79 μm in rubidium. Listed in Tables 2.2-2.4 are a number of properties useful in the analysis of the data. The stimulated emission cross sections calculated in Table 2.3 were found using Equation 2.1,

$$\sigma_{21} = \frac{A_{21}\lambda_{21}^2}{8\pi n^2} g(\nu_{21}), \tag{2.1}$$

where σ_{21} is the stimulated emission cross section for a transition from a higher to lower energy state, A_{21} is the Einstein A coefficient, λ_{21} is the associated laser wavelength, n is the index of refraction (taken to be 1), and $g(\nu_{21})$ is the Doppler line shape at line center.

Table 2.2: Fundamental constants

Fundamental constants	
c = Speed of Light	2.99792458×10^{8} m/s
h = Planck's constant	$6.62606957 \times 10^{-34}$ J-s
k = Boltzmann constant	$1.3806488 \times 10^{-23}$ J/K
Avogadro's number	$6.02214129 \times 10^{23}$ /mole
π = pi	3.14159265

Table 2.3: Einstein A coefficients and stimulated emission cross sections for rubidium

Rubidium Transition	A Coefficient (s^{-1})	Stimulated Emission Cross Section (cm^2)	Energy Difference (cm^{-1})
$5P_{3/2}$-$5S_{1/2}$	3.81×10^{7}	1.35×10^{-11}	12816.54
$5P_{1/2}$-$5S_{1/2}$	3.61×10^{7}	1.4×10^{-11}	12578.95
$6P_{3/2}$-$5S_{1/2}$	1.77×10^{6}	9.83×10^{-11}	23792.59
$6P_{1/2}$-$5S_{1/2}$	1.5×10^{6}	2.52×10^{-11}	20132.51
$6P_{3/2}$-$6S_{1/2}$	4.63×10^{6}	7.76×10^{-11}	3660.08
$6P_{1/2}$-$6S_{1/2}$	4.4×10^{6}	7.91×10^{-11}	3582.57

Table 2.4: Relevant experimental values discussed in sections III and IV

Experimental Conditions	
t_p = Pump Pulse Duration	10 ns
f_p = Pump Pulse Repetition Rate	10 Hz
l_p = Pump Laser Linewidth	0.05 cm^{-1}
A_{laser} = Pump Laser Spot Size	7.1 mm^2
V_p = Pump Volume	0.923 cm^3
l_g = Gain Length	13 cm
τ_{cl} = Photon Cavity Lifetime	4.33 x 10^{-10} s
I_{avg} = Average Instantaneous Pump Intensity	5 MW/cm^2
$I_{s2.73\mu m} = 6P_{1/2}$-$6S_{1/2}$ Saturation Intensity	4.0 x 10^{-3} W/cm^2
$I_{s2.79\mu m} = 6P_{3/2}$-$6S_{1/2}$ Saturation Intensity	4.3 x 10^{-3} W/cm^2
1st Ionization Potential	33690.81 cm^{-1}
n_{Rb} = Rb Number Density	6.5x$10^{13}$$cm^{-3}$ - 5.2 x$10^{14}$$cm^{-3}$
γ_o = Calculated Small Signal Gain	2522 cm^{-1} - 20566 cm^{-1}
t_{pb} = Calculated Photon Buildup Time	3.24 x 10^{-12}s - 2.64 x 10^{-11}s
Cell Window Transmission	85%
P_{loss} = Total Pump Power Loss	~50%

III. Experimental Setup

Chapter Overview

This chapter explores the experimental setup and techniques used to analyze the effects various parameters had on the stimulated emission of the $6^2P_{3/2}$-$6^2S_{1/2}$ and $6^2P_{1/2}$-$6^2S_{1/2}$ transitions in rubidium vapor. After determining which energy transitions produced observable lasing for a given optical pump, laser excitation spectra and spot size and divergence were measured, as well as the effect pump power, rubidium concentration, and the presence of argon, ethane, and helium had on laser output.

Experimental Setup

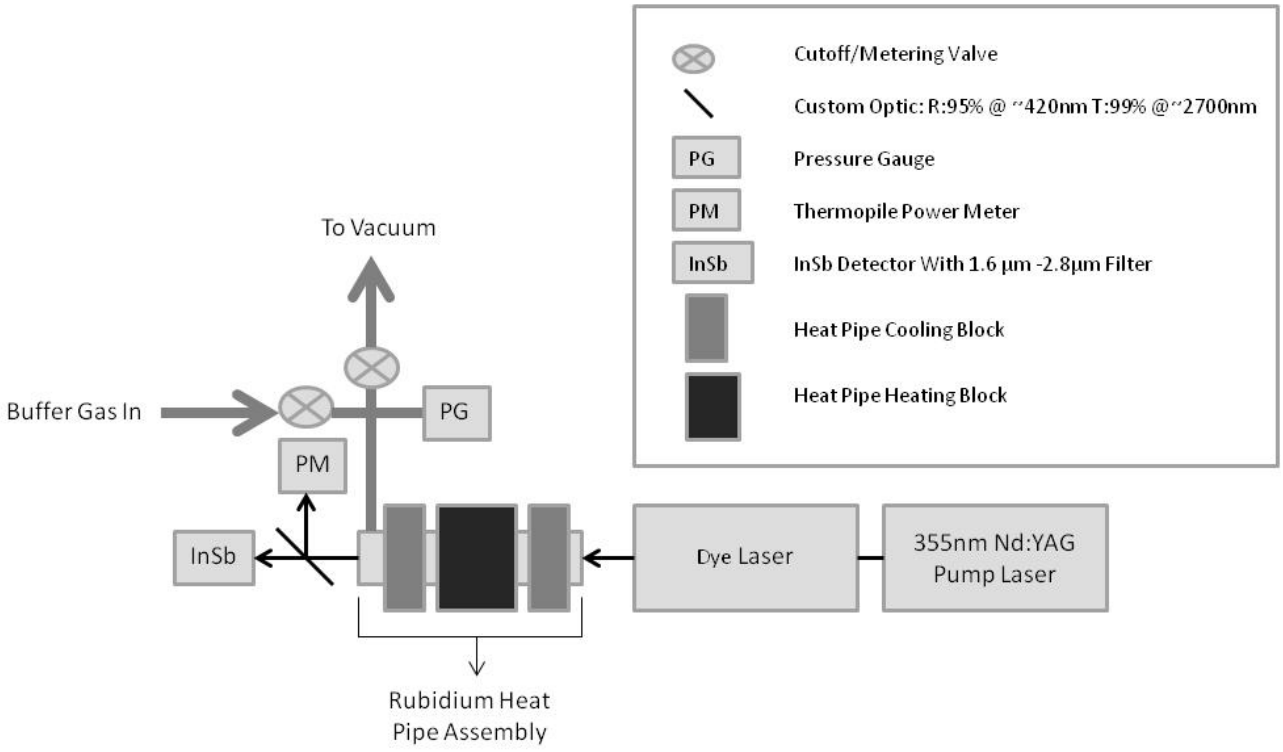

Figure 3.1: Experimental setup.

A Continuum Surelite frequency tripled Nd:YAG laser was used to pump a Continuum ND6000 dye laser circulating Stilbene 420 laser dye (Exciton, Inc. S-420). The dye was tunable from 412-444 nm providing a suitable means to obtain the 420.2 nm and 421.7 nm pump wavelengths necessary for laser excitation. The dye's lifetime was very short, however, providing a half-life of just 15 minutes. The dye laser had a 0.05 cm^{-1} linewidth, 10 ns full width at half max pulse width, and was operated at a repetition rate of 10 Hz. Dye laser output power was controlled by varying the Q-switch timing of the Nd:YAG laser, allowing pulse energies up to ~10 mJ. The output beam of the dye laser was ~5 mm in diameter, although the majority of the energy was concentrated in a crescent shape as shown in the laser burn of Figure 3.2. This resulted in pump intensities of up to ~5 MW/cm^2. The pump beam was normally incident on a sapphire window on the front of the heat pipe as shown in Figure 3.1.

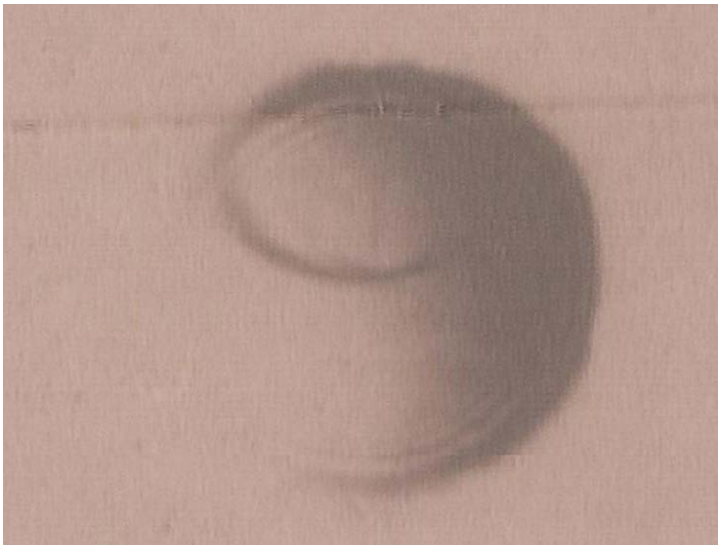

Figure 3.2: ~5mm diameter pump laser burn at ~5 mJ/pulse.

The heat pipe consisted of a 25.4 cm long, 2.54 cm diameter stainless steel tube with flanges welded to both ends to hold the sapphire windows (Klennert, 2012). A 10.2 cm long heating block, which accepted 8 Watlow brand cartridge heaters, was clamped on the center of the tube allowing for temperatures up to 190 ˚C. The cartridge heaters maintained their temperature by referencing a thermocouple that was attached to the outside of the heating block. Similar to the heating block, two cooling blocks were clamped 1.27 cm away from the edges of the heater block on both sides. These cooling blocks circulated a water flow past the tube at a temperature of 20 ˚C, which was maintained by a Neslab RTE-111 recirculating chiller. On the inside of the heat pipe tube was a 150 x 150 wire/inch stainless steel mesh compressed against the inside walls by a stainless steel spring. One gram of rubidium was placed inside the center of the tube in the middle of the heated segment. When the heater block was sufficiently hot (+100 ˚C) the rubidium evaporated and moved down a temperature gradient toward the cooled segments where it condensed and underwent a wicking action via the mesh back toward the heated segment. The continuation of this process maintained constant alkali concentration and an effective gain path length of 13 cm. Heater block temperatures ranged from 145 ˚C – 190 ˚C, which based on equation 3.1 produced rubidium number densities of 6.5 x 10^{13} cm^{-3} to 5.2 x 10^{14} cm^{-3} (Steck, 2008:3).

$$\mathrm{Log}_{10}[P_v] = -15.88253 - \frac{4529.635}{T} + 0.00058663T - 2.99138\mathrm{Log}_{10}[T], \qquad (3.1)$$

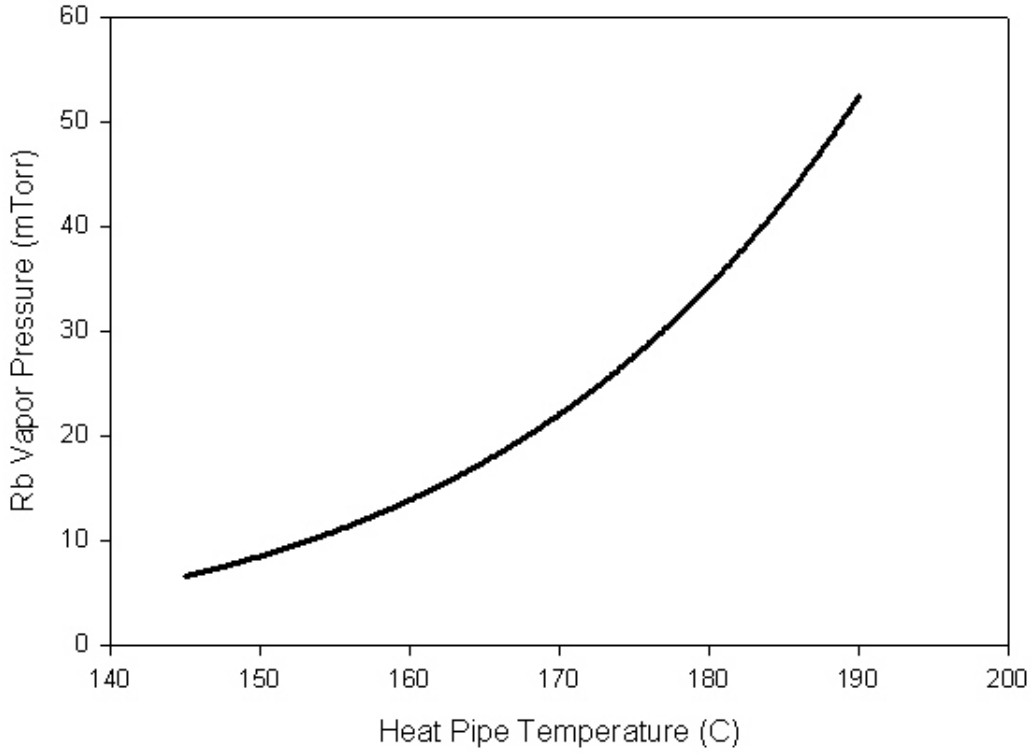

Figure 3.3: Rubidium vapor pressure vs. associated heat pipe temperature.

It is seen that temperature changes of 10-20 ˚C change Rb number density by a factor of ~1-2. Therefore, the Rb temperature must be well known to prevent significant errors that can arise in future calculations. As will be discussed later, equating the rubidium temperature to that of the heater block sensed by the thermocouple may not be a great assumption, thus impacting quantitative analysis.

Following the heat pipe exit was a custom coated optic designed to reflect +95% of ~420 nm light incident at 45 degrees, and transmit +99% of ~2700 nm light incident at 45 degrees. This allowed for the removal of the pump beam from the IR signals of interest. The IR emission was incident on a liquid nitrogen cooled InSb detector with a

1.6-2.8 μm bandpass filter. The InSb output signal was read by a 1 GHz LeCroy Wavepro 7100 digital oscilloscope and the area under each pulse was integrated for a single value. In order to convert this value to the pulse energy of the IR signal, a black body calibration was conducted, which will be discussed later.

In order to monitor input pulse energy, a Coherent Field Max II thermopile power meter was used. First, however, determining a relationship between the pump powers measured before and after the heat pipe was necessary. This allowed the power meter to stay behind the heat pipe, eliminating the need to repeatedly remove and replace it from in front of the heat pipe to monitor power. This proved especially important since the degradation of the dye was at times significant over the course of an experiment. More focus, therefore, was able to be placed on actively controlling the input power. The incident to transmitted pump power ratio going into and coming out of the heat pipe showed losses between 40% - 60%. It was generally considered that twice the energy measured at the heat pipe exit was incident on the entrance. In order to determine how much of the incident pump power was absorbed by the rubidium, the transmitted vs. incident pump power was measured when the dye laser was both on and off resonance. These measurements were taken at heat pipe temperatures of 33 $^{\circ}$C, 145 $^{\circ}$C, 160 $^{\circ}$C, 175 $^{\circ}$C, and 190 $^{\circ}$C, using three different pump powers for each case. The collective averages and standard deviations of these ratios showed effectively no absorption. The results actually showed a ~0.01% increase in signal, although there was a ~3.5% error bound.

Both the vapor pressure of rubidium and the pressure of the buffer gasses were monitored and controlled with metering and cutoff valves, MKS capacitance manometers, and an Alcatel vacuum pump that could maintain vacuum as low as 10 mTorr.

Spectroscopic Determination of Lasing Transitions

In order to determine which signals may be observable, a TRIAX 320 monochrometer was scanned over a wavelength range of ~1.5-3.5 μm of an Electro-Optical Systems liquid nitrogen cooled InSb detector with 2mm diameter active area. The TRIAX 320 contained 600 groove/mm and 300 groove/mm gratings, blazed at 1500 nm and 4000 nm respectively, which were both used to confirm the signals present. The only observable signals were at 2.73 μm when the Rubidium vapor was pumped at 420.2 nm, and 2.79 μm when pumped at 421.7 nm. This determination allowed for the independent study of the effect various parameters had on the given IR signal strength.

Laser Excitation Spectra

The laser excitation spectra of the 2.73 μm and 2.79 μm IR lines were obtained by scanning the pump laser over 200 pm at a 10 pm step size of the $5^2S_{1/2}$–$6^2P_{3/2}$ and $5^2S_{1/2}$–$6^2P_{1/2}$ absorption profiles. With a heat pipe temperature of 160 ˚C, and resulting rubidium vapor number density of 1.4×10^{14} cm^{-3}, IR signals were measured with a Judson InSb detector with a 1.6-2.8 μm bandpass filter, 2 mm diameter active area, and ~150 ns rise time. The maximum output energy was found for each scan through the absorption

profile and the dye laser wavelength was calibrated accordingly for all of the following work.

Spot Size of Lasing Emission

Using the pump wavelengths at peak absorption, IR beam spot sizes were found. A 0.5 mm slit was translated across the cross section of each respective IR beam at ~25 cm from the heat pipe exit. Each IR beam had an approximate diameter of 3.5 mm matching the energy distribution of the pump beam shown in Figure 3.2 fairly well.

Lasing Intensity vs. Pump Power and Rb Concentration

The IR output energy of each line was measured at four pump energies at four different heat pipe temperatures and rubidium concentrations. Temperatures of 145 $^{\circ}$C, 160 $^{\circ}$C, 175 $^{\circ}$C, and 190 $^{\circ}$C were used, corresponding to Rb concentrations of 6.5×10^{13} cm^{-3}, 1.4×10^{14} cm^{-3}, 2.8×10^{14} cm^{-3}, and 5.2×10^{14} cm^{-3} respectively. At each of these concentrations transmitted pump energies of ~0.4 mJ, 1 mJ, 2 mJ, and 3 mJ were used. These pump energies were determined by measuring the transmitted pump laser output as a continuous wave source, and dividing by its repetition rate.

Effects of Buffer Gas Concentration

The effect argon, ethane, and helium had on IR output were individually studied for a heat pipe temperature of 190 $^{\circ}$C and rubidium concentration of 5.2×10^{14} cm^{-3}. The heat pipe was initially evacuated to ~10 mTorr by the Alcatel vacuum pump before it was sealed off and heated. Upon reaching 190 $^{\circ}$C, a small flow of buffer gas of about one Torr

per five seconds was introduced by means of a needling valve, while the rubidium vapor was pumped at ~2.5 mJ input pump pulse energy. Buffer gas was then allowed to increase until well past the point that it was evident IR signal was fully quenched.

Black Body Calibration

In order to convert the IR output signal measured on the oscilloscope to pulse energy, a black body calibration was conducted. The black body source used was from Electro-Optical Industries (Model # CS1050-100) with a temperature range up to 1000 ˚C. Eight circular aperture sizes were available, and diameters of 0.5 mm, 1.58 mm, and 4 mm were used. The aperture was placed a distance of 5 cm and 10 cm away from the InSb detector described above, and signal strength was observed at 600 ˚C, 700 ˚C, and 800 ˚C at each aperture size. This provided 18 values of signal strength corresponding to known radiometric conditions.

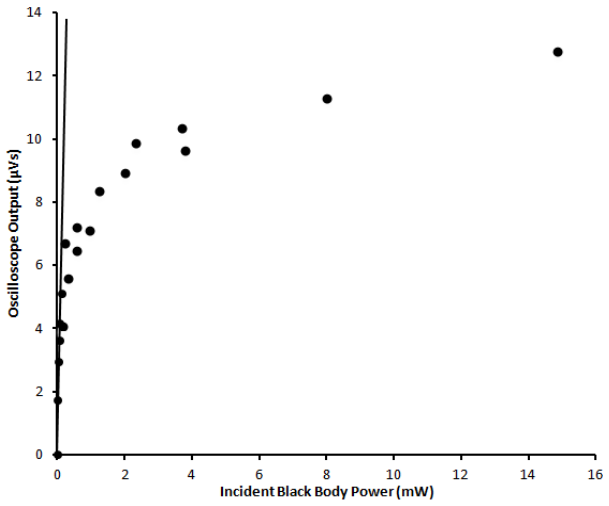

Figure 3.4: Oscilloscope response to incident black body power.

The spectral radiance of a black body source is given by,

$$L = \frac{2\mathrm{hc}^2}{\lambda^5(e^{\frac{\mathrm{hc}}{\lambda \mathrm{kT}}} - 1)}, \tag{3.2}$$

In order to find the power incident on the detector, equation 3.2 was integrated for each scenario over 1.6-2.8 μm matching the detectivity range of the InSb detector,

$$P = \int_{1.6\mu\mathrm{m}}^{2.8\mu\mathrm{m}} \left(\frac{A_s A_d}{R^2 \pi}\right)\left(\frac{2\mathrm{hc}^2}{\lambda^5(e^{\frac{\mathrm{hc}}{\lambda \mathrm{kT}}} - 1)}\right) d\lambda, \tag{3.3}$$

where A_s is the blackbody aperture area, A_d the detector area, R the distance between the detector and blackbody aperture, h the Planck constant, c the speed of light, k the Boltzmann constant, and T the temperature of the black body. It can be seen in Figure 3.4 that the responsivity of the detector is very nonlinear outside of the first 6-7 data points. Since, however, the oscilloscope output for the IR data was well within the linear region, a linear fit was made relating oscilloscope output to incident power (53.1 μVs/mW). This allowed the calculation of IR pulse energy from the measured oscilloscope output.

IV. Results

Chapter Overview

This chapter will focus on the experimental results from the tests outlined in Section III. As an aid to analyze the interesting features of the data, two scenarios of a simplified model are presented. A discussion of sources of uncertainty is also included.

Laser Excitation Spectra

Figure 4.1 shows the laser excitation spectra for the absorption profiles peaked at 420.2 nm and 421.7 nm. Gaussian curves of the form,

$$A\exp(-B(\lambda - C)^2) \tag{4.1}$$

were fit to the emitted IR pulse energy as a function of pump laser wavelength data, which was sampled at 10 pm step sizes.

Table 4.1: Laser Excitation Fit Parameters

Infrared Emission	A	B	C
2.73 μm	3.85	0.22	420.2
2.79 μm	3.34	0.14	421.7

Using these equations, full width at half max values for each absorption profile were found, and are shown in Figure 4.1 Also listed are the respective spontaneous emission A coefficients.

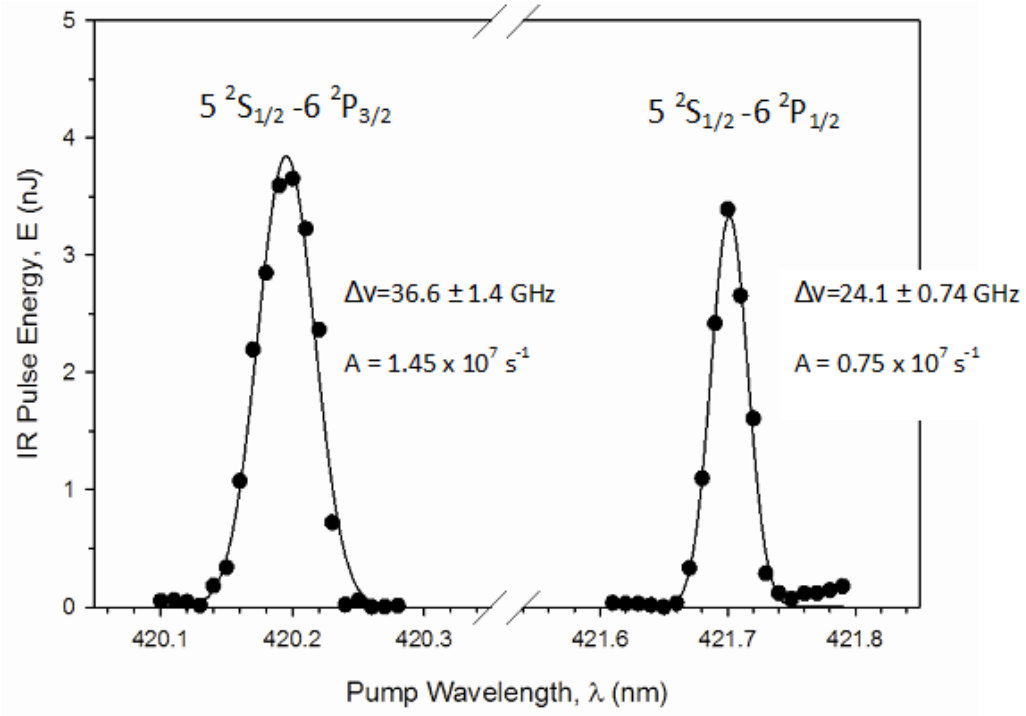

Figure 4.1: Laser excitation spectra in 1.4 x 10^{14} cm^{-3} Rb vapor optically pumped at 0.4 mJ.

The pump transitions have a Doppler width of ~1.2 GHz, but as shown in Figure 4.1, 24 GHz - 36GHz were observed. This can be partially explained by the large degree of power broadening occurring in the system. In order to confirm this, power broadened full width at half max values were approximated using equation 4.2,

$$\Delta\nu = \frac{A_{32}}{2\pi}\sqrt{1+\frac{I}{I_{\text{sat}}}}, \tag{4.2}$$

where A_{32} is the spontaneous emission rate for the lasing transition from either $6P_{3/2}$-$6S_{1/2}$ or $6P_{1/2}$-$6S_{1/2}$, I is the pump intensity, and I_{sat} is found using equation 4.3.

$$I_{\text{sat}} = \frac{h\nu_{32}(A_{32}+A_{30})}{\sigma_{32}}, \tag{4.3}$$

where ν_{32} is the lasing frequency, A_{30} the spontaneous emission rate from the $6P_{3/2}$-$5S_{1/2}$ or $6P_{1/2}$-$5S_{1/2}$ states, and σ_{32} the stimulated emission cross section for the lasing transition. Although this equation is for homogenous broadening, in the large hole limit of a high intensity pump, such as is the case here, it still holds for this inhomogenously broadened system. The results of equation 4.5 give power broadened widths of 5.1 GHz and 7.1 GHz for the respective $6P_{1/2}$-$6S_{1/2}$ and $6P_{3/2}$-$6S_{1/2}$ transitions. The ratio between the two calculated transition widths (.71) compared to that of the two measured widths (.66) agree well. The difference between the two can be accounted for by making a slight adjustment to the uncertain 7.1 mm^2 area used when determining pump intensity I. It can also be seen that the ~30% larger line shape of the $6^2P_{3/2}$-$5^2S_{1/2}$ transition when compared to the $6^2P_{1/2}$-$6^2S_{1/2}$ transition is a direct result of the difference in stimulated emission cross section between the two transitions.

Lasing Intensity vs. Pump Power and Rb Concentration

The energy per pulse in the infrared beams of the $6^2P_{3/2}$ and $6^2P_{1/2}$ pump states is shown as a function of pump energy per pulse in Figures 4.2 and 4.3 at the four different rubidium concentrations listed in Section III. Curves were fit to the data of the form,

$$E=E_m(1-\exp(\eta(E_p-E_{th})/E_m)), \qquad (4.4)$$

where E = IR pulse energy, E_m = bleached limit (maximum output energy), η = slope efficiency, E_p =transmitted pump energy, and E_{th}=threshold pump energy. Values for these fit parameters are listed in Table 4.2. Threshold is achieved in all cases with only a small fraction of the pump energy available. Initially the energy of the IR emission rises quickly, but saturates at pump energies exceeding ~1mJ limiting the output to about 5 nJ/pulse, or 50 nW average power. The figure also illustrates the change in performance with increasing rubidium concentration. At the highest pump energies, the IR energy initially increases with rubidium concentration, but reaches a limiting value for concentrations exceeding ~ 3 x 10^{14} cm^{-3}.

Table 4.2: Fit parameters for IR signal vs. pump power and Rb concentration

Rb Concentration	E_m=Bleached Limit (nJ)		E_{th}=Threshold Pump Energy (mJ)		Slope Efficiency (10^6 η)	
($10^{13}cm^{-3}$)	$6P_{3/2}$-$6S_{1/2}$	$6P_{1/2}$-$6S_{1/2}$	$6P_{3/2}$-$6S_{1/2}$	$6P_{1/2}$-$6S_{1/2}$	$6P_{3/2}$-$6S_{1/2}$	$6P_{1/2}$-$6S_{1/2}$
6.5	3.27	2.77	0.11	0.17	11	3.22
13.7	4.51	4.23	0.1	0.34	12.3	12
27.4	4.84	4.56	0.04	0.21	40.1	46.2
52.1	4.75	4.68	0.14	0.37	96.7	1

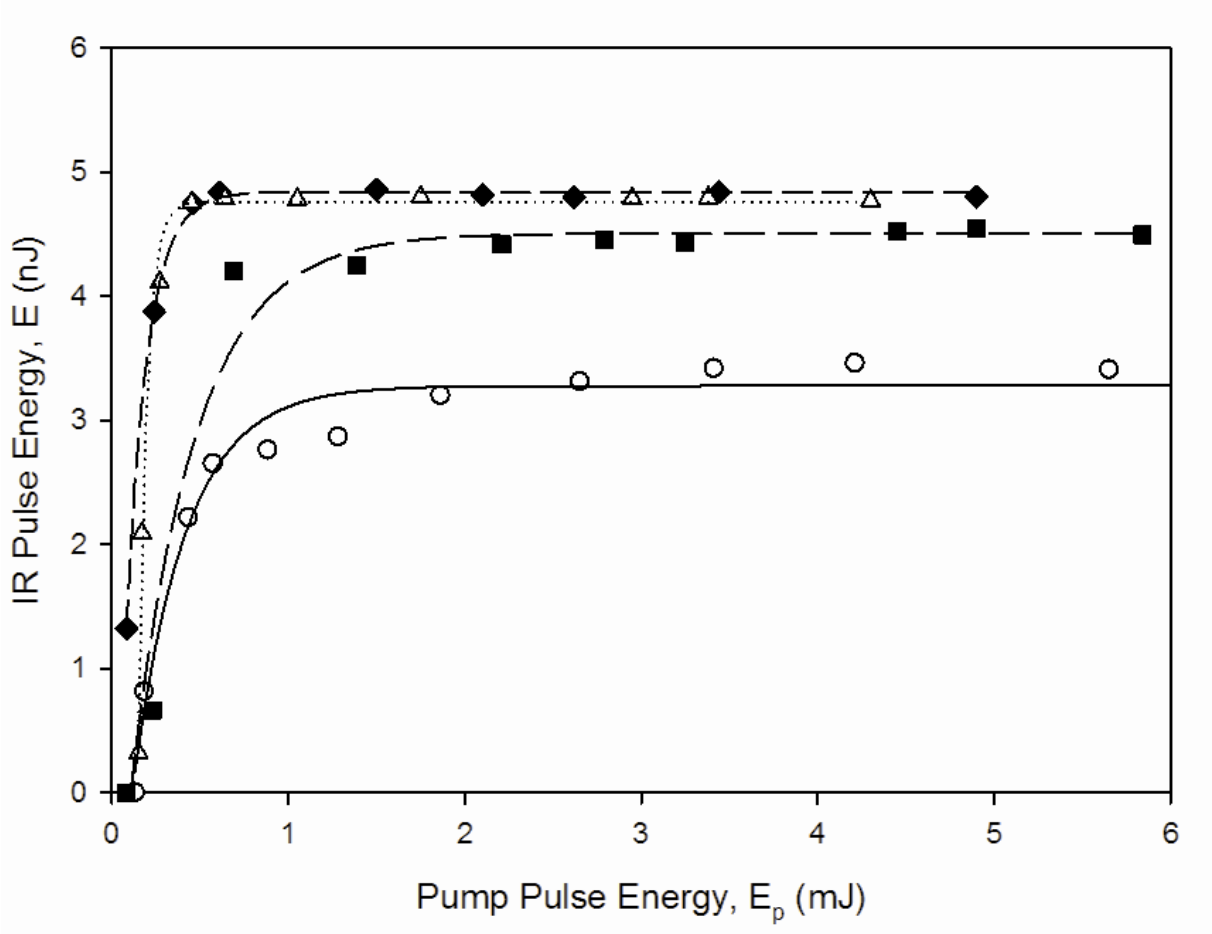

Figure 4.2: IR pulse energy vs. transmitted pump energy at 2.73 μm pumped at 420.2 nm for four different Rb concentrations. ○ = 6.5×10^{13} cm^{-3}, ■ = 1.4×10^{14} cm^{-3}, Δ = 2.8×10^{14} cm^{-3}, ♦ = 5.2×10^{14} cm^{-3}

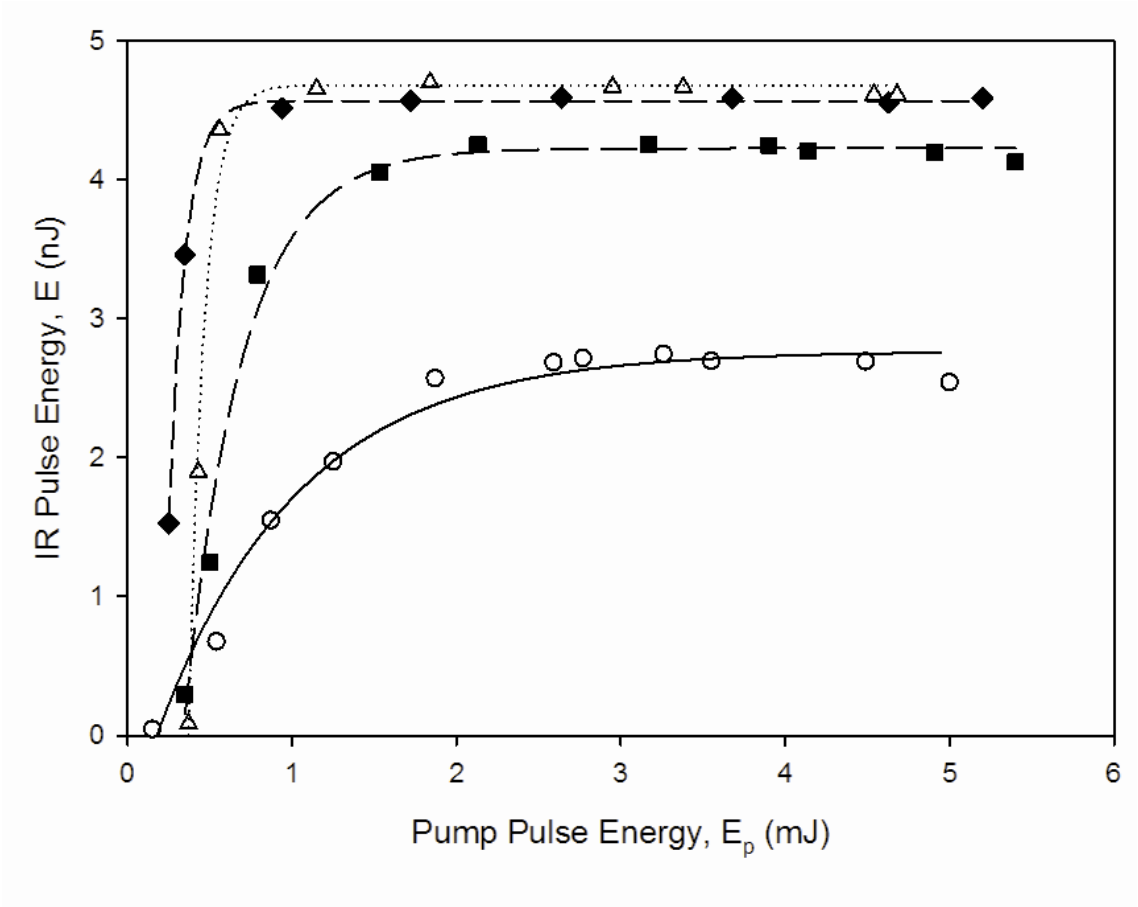

Figure 4.3: IR pulse energy vs. transmitted pump energy at 2.79 μm pumped at 421.7 nm for four different Rb concentrations. ○ = 6.5×10^{13} cm^{-3}, ■ = 1.4×10^{14} cm^{-3}, Δ = 2.8×10^{14} cm^{-3}, ♦ = 5.2385×10^{14} cm^{-3}

Figure 4.4 shows the threshold energy as a function of rubidium number density. While all threshold energies are small, there is clearly no correlation among the data. The slope efficiency vs. number density plot shown in Figure 4.5 does, however, show a linear trend, with the exception of the final data points, as the slope efficiency increases with increasing rubidium concentration. Figure 4.6 further shows the asymptotic behavior of the bleached limit as the IR emissions initially rises linearly, but the curve starts to roll over to a limiting value as rubidium number density is increased.

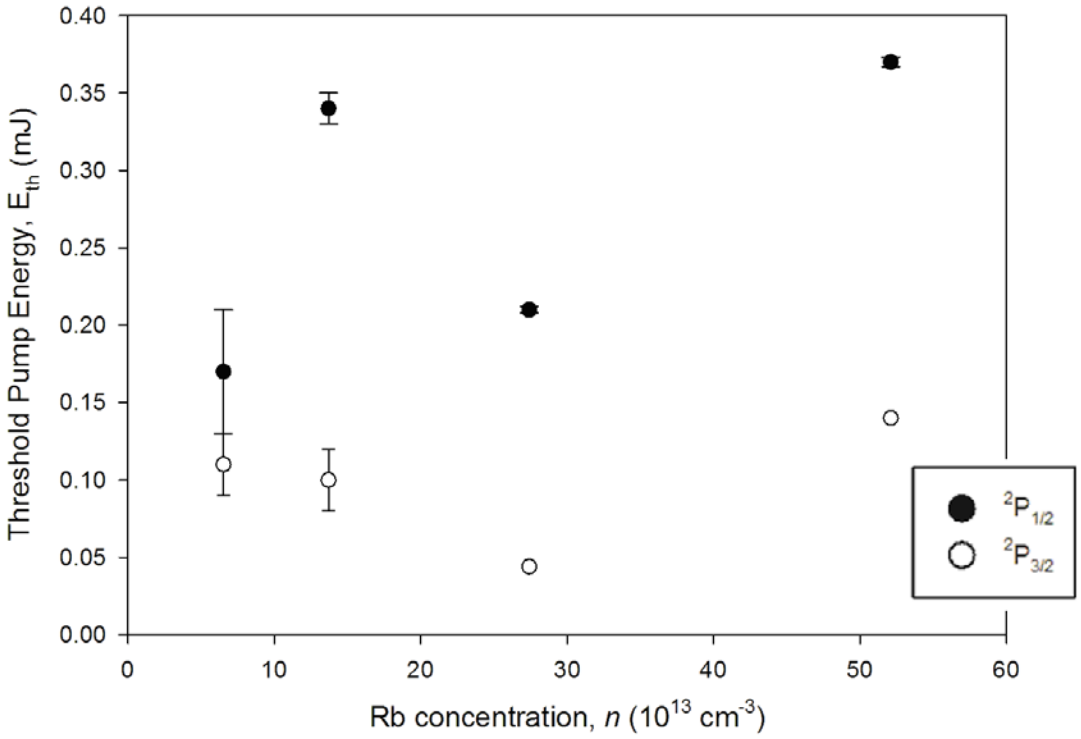

Figure 4.4 Threshold pump energy vs. rubidium concentration

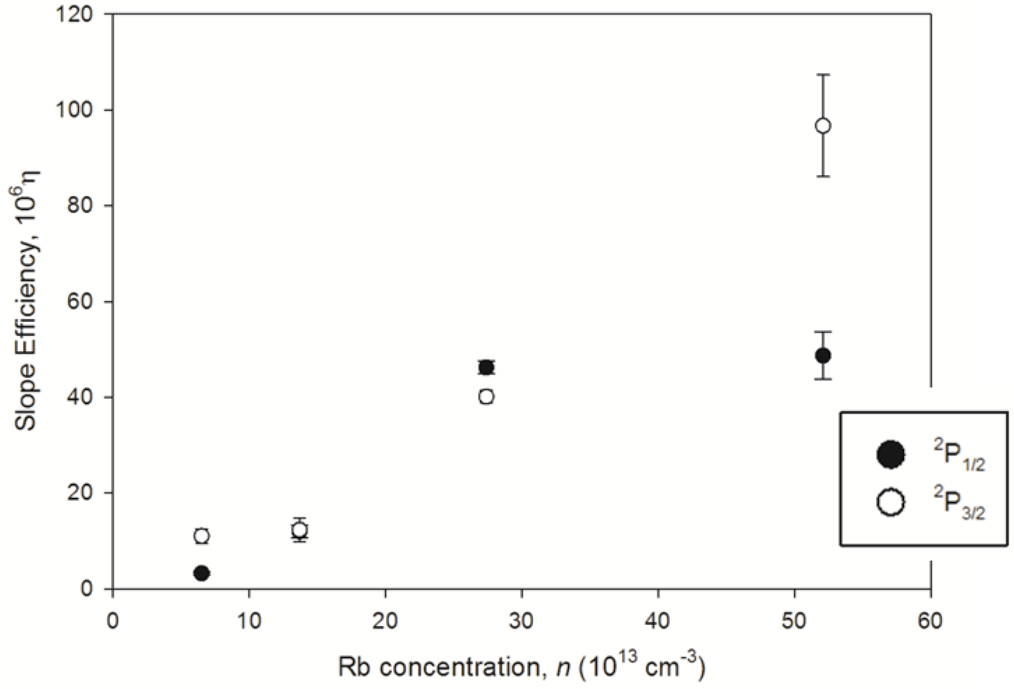

Figure 4.5: Slope efficiency vs. rubidium concentration

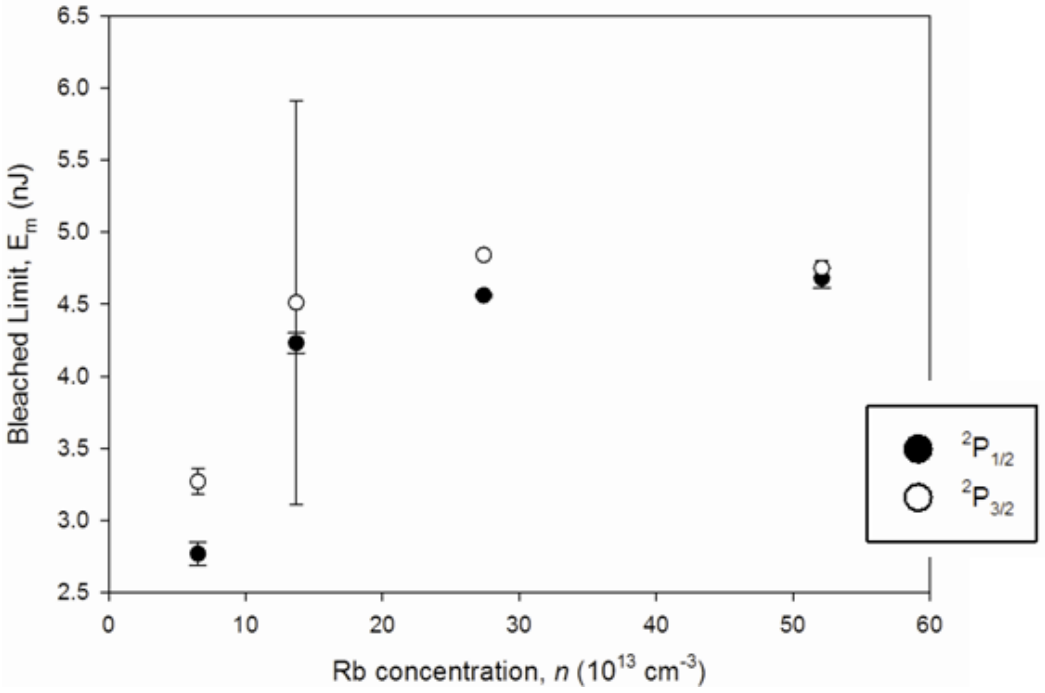

Figure 4.6: Bleached limit vs. rubidium concentration

It is seen Figure 4.7, using a pulse energy in the bleached limit of 4 mJ, IR pulse energy vs. rubidium concentration scales linearly for low rubidium concentration. Overlaid on top of this data is the corresponding work done by Sharma (Sharma, 1981:209). Due to the fact Sharma's gain length was different, however, a scaling factor of 8.8 was applied to his data for the data sets to overlap. Intuitively, the IR signal should increase with rubidium number density at pump energies beyond the bleached limit, but after around a $3x10^{14}cm^{-3}$ concentration of rubidium, this trend stops. It is shown in Sharma's data that the IR signal actually begins to decrease at higher rubidium concentrations, and it is expected the data in this study would show similar trends if higher rubidium concentrations were analyzed. It can be proposed the decrease in lasing at higher rubidium concentrations is due to multi-photon events and ionization (Lucatorto, 1980:3948).

Lucatorto proposed a number of mechanisms for ionization in dense atomic vapor outside of multi-photon ionization among isolated atomic atoms and dimers. Much analysis has been conducted on sodium systems, which will be used here to help shed light on the processes occurring in the rubidium system under investigation. A first consideration is the energy pooling that occurs when two excited atoms collide with the possibility one transfers its energy to the other. Then, in the presence of the pump laser, photoionization occurs. A calculation was done to estimate the absolute cross section in sodium for the 3p-4d transition (Kowalczyk,1979:203) which Lucatorto interpolated for work he conducted to get a result of $\sigma_{3p4d} = 7.4 \times 10^{-16}$ cm^2 (Lucatorto, 1976:428). He then used this to estimate the absolute cross sections $\sigma_{3p3d} = 8.5 \times 10^{-15}$ cm^2,

σ_{3p4p} = 3.0 x 10^{-16} cm^2, σ_{3p5s} = 7.4 x 10^{-16} cm^2, σ_{3p6s} = 1.2 x 10^{-17} cm^2, and σ_{3p5d} = 2.5 x 10^{-17} cm^2.

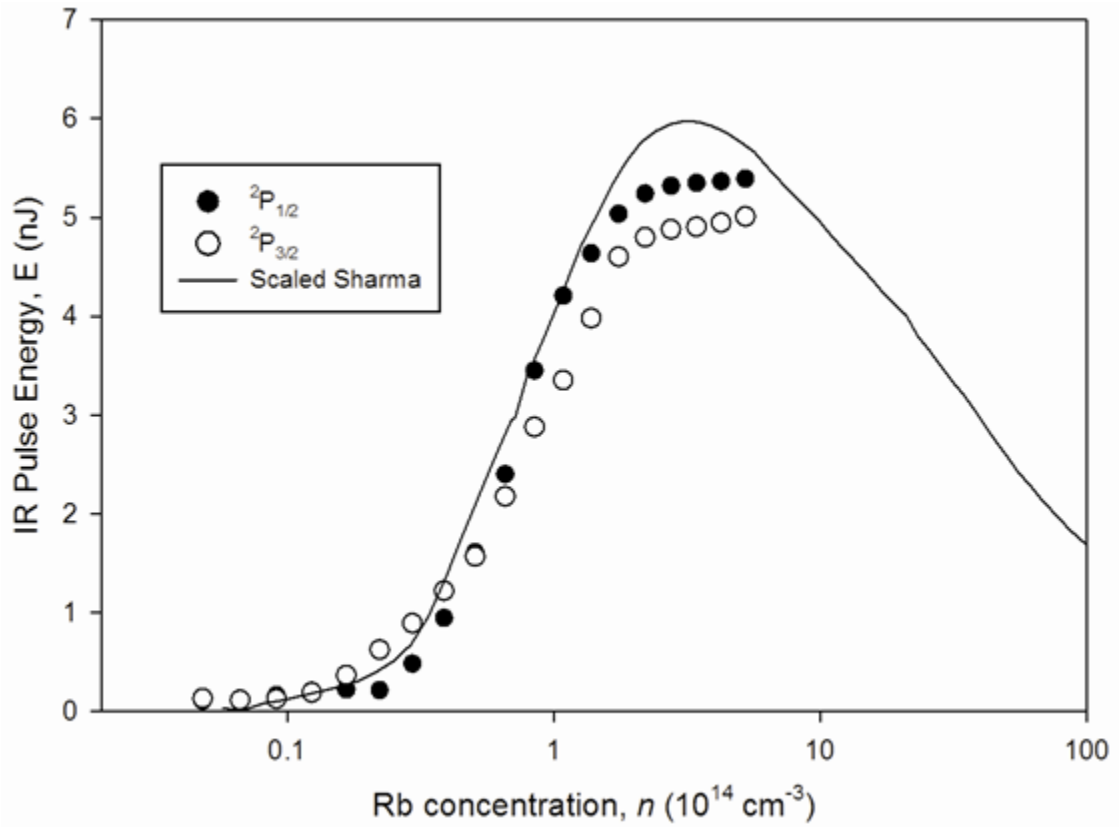

Figure 4.7: Output pulse energy vs. Rb concentration at 2.73 μm (●) and 2.79 μm (○) when pumped at 420.2 nm and 421.7 nm respectively.

All states above the 3p level in sodium can be ionized with a 589.6 nm pump laser. A measurement of the ionization cross section was conducted for the 4s and 5d states in sodium yielding σ_{4s} = 15.2 x 10^{-18} cm^2, and σ_{5s} = 1.5 x 10^{-18} cm^2 (Smith, 1980:577). If it is assumed no other processes are occurring, this yields ~10% ionization. The energies

vary from atom to atom, however, and the number of states that are accessible for ionization determines the degree to which the vapor is ionized.

Associative ionization may also occur where two excited atoms collide resulting in the formation of an auotionizing dimer. The cross section for this process in sodium has been measured to be up to 10 x 10^{-16} cm^2 (Bearman, 1978:1227) which results in ~20% ionization in Lucatorto's work. This cross section has also been measured in rubidium to be 1.6 x 10^{-16} cm^2 (Borodin, 1975:201).

Another proposed mechanism is for an atom to simultaneously absorb energy from the laser and collide with another excited atom. The cross section for this process has been measured in sodium to be 10 x 10^{-16} cm^2 (Polak-Dingles, 1980:1663), which would result in ~0.01% ionization in Lucatorto's work.

Finally, stimulated Raman scattering also has the potential to populate higher energy states that are subject to photoionization, which in Lucatorto's estimate would, neglecting competing processes, contribute to ~10% ionization in sodium.

Effects of Buffer Gas Concentration

Figures 4.8 and 4.9 show the IR emission of rubidium vapor at 5.2 x10^{14} cm^{-3} in `the presence of an individual buffer gas of argon, ethane, or helium. Both the $6P_{3/2}$-$6S_{1/2}$ and the $6P_{1/2}$-$6S_{1/2}$ transitions were fully quenched at less than 50 Torr of buffer gas. Argon proved the least effective quencher of the three gases, but still fully quenched the $6P_{3/2}$-$6S_{1/2}$ transition at ~45Torr and the $6P_{1/2}$-$6S_{1/2}$ transition at ~27 Torr. Ethane and helium proved to have a similar effect in quenching the $6P_{3/2}$-$6S_{1/2}$ transition at ~15Torr and the $6P_{1/2}$-$6S_{1/2}$ transition at ~7Torr. The $6P_{1/2}$-$6S_{1/2}$ transition also became fully

quenched at approximately twice the rate of the $6P_{3/2}$-$6S_{1/2}$ transition. The odd nature of the plots for the first few Torr, especially shown with argon, can be attributed by the nature in which the buffer gases entered the heat pipe. The heat pipe was initially isolated from the vacuum system, and contained only the rubidium vapor at a couple of tens of mTorr. The buffer gas entrance rate was then set up to enter the heat pipe at ~1 Torr every 5 seconds. Once this rate was established a valve on the heat pipe was opened creating an initially unstable environment. After the first few Torr of gas filled the heat pipe, the plots show a more consistent trend as further buffer gas was added.

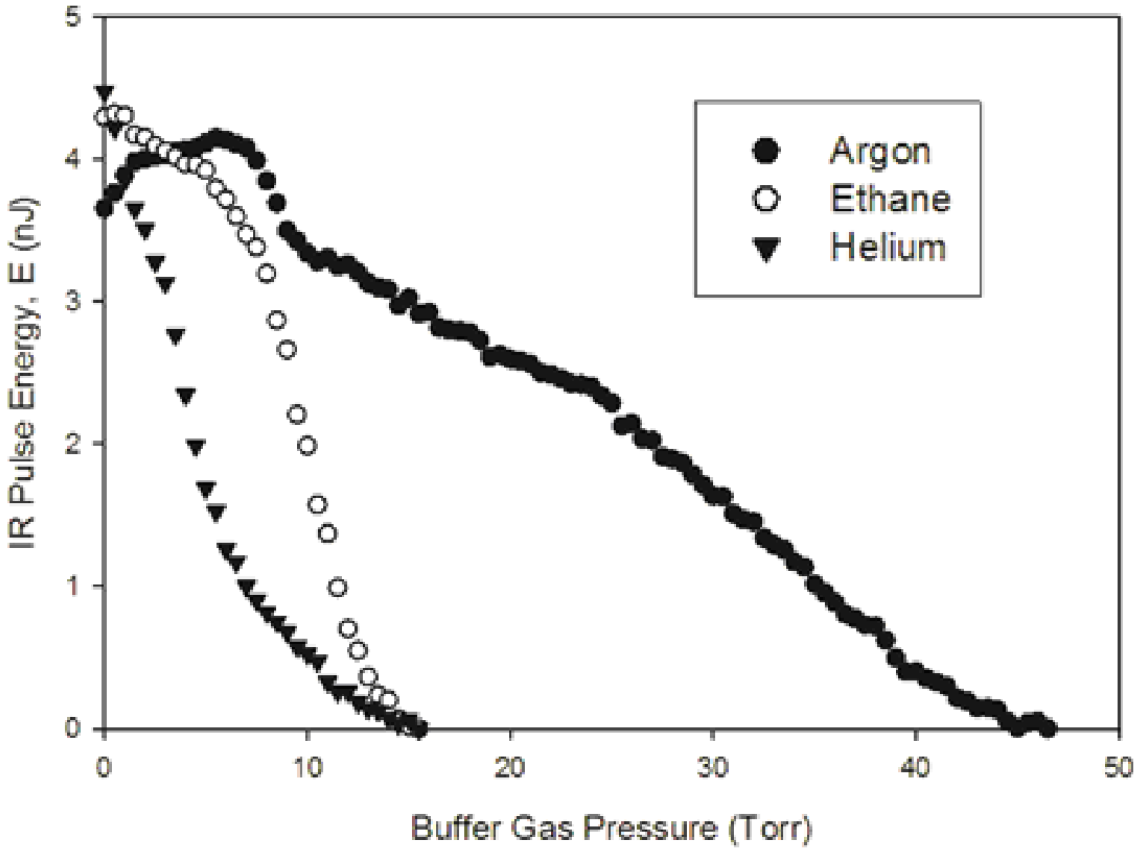

Figure 4.8: Output pulse energy at 2.73 μm vs. buffer gas pressure when pumped at 420.2 nm.

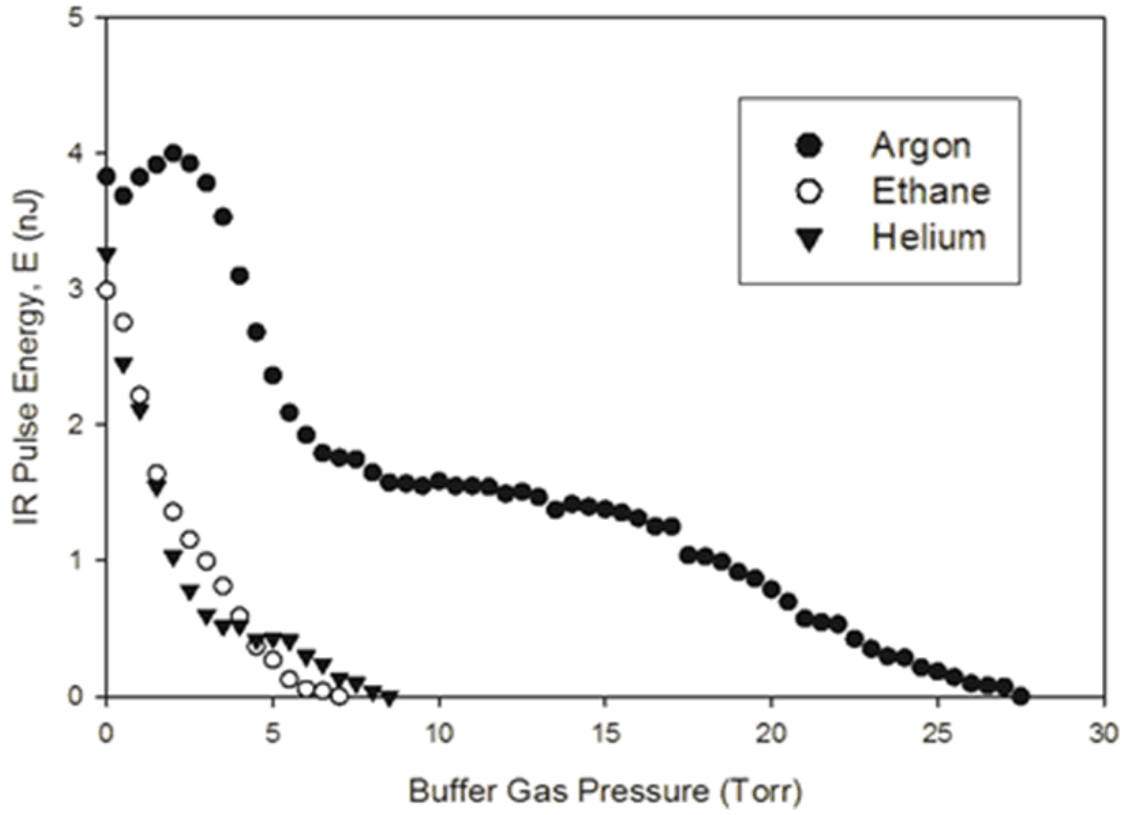

Figure 4.9: Output pulse energy at 2.79 μm vs. buffer gas pressure when pumped at 421.7 nm.

The cross section for each of the buffer gases was calculated with equations 4.5 and 4.6. In order to find these values, the concentration of each buffer gas, [BG], was first determined at the pressure where the emission along the $6P_{3/2}$ or $6P_{1/2}$ to $6S_{1/2}$ was comparable to the deactivation of the $6P_{3/2}$ or $6P_{1/2}$ to all other states. The average speed, g, of each buffer gas was found at 190 ˚C, and with the pump pulse width t_p, the buffer gas cross section, σ_{BG} was found.

$$g = \sqrt{\frac{8\mathrm{kT}}{\pi \mathrm{m_{BG}}}}, \tag{4.5}$$

$$\sigma_{\mathrm{BG}} = \frac{1}{g[\mathrm{BG}]t_p}, \tag{4.6}$$

where k is the Boltzmann constant, T the temperature of the buffer gas and rubidium vapor, and m_{BG} the atomic mass of each buffer gas. For the 2.73 μm emission, the cross sections for argon, helium, and ethane were 51, 82, and 109 nm^2, respectively. For the 2.79 μm emission, the cross sections were 126, 135, and 372 nm^2. While these values are excessively large and not intended to count as cross section measurements, they do depict the rapid collisional deactivation observed for both transitions.

Very little has been reported for comparison about the quenching cross section of the second lowest $^2P_{3/2}$ or $^2P_{1/2}$ states in rubidium, but there have been measurements of the quenching cross section of these states in cesium using ethane and helium (Brown, 2012:40). This experiment measured quenching cross sections at the second lowest $^2P_{3/2}$ in ethane and helium at 80 $Å^2$ and 5 $Å^2$, respectively, and 10 $Å^2$ and 1 $Å^2$ for the second lowest $^2P_{1/2}$ state. These values are about four orders of magnitude less than what is calculated here for the analogous rubidium case, suggesting much higher quenching cross sections.

Model

Both scenarios considered here consist of three states as shown in Figure 4.1. State 0 is the $5S_{1/2}$ ground state, state 3 is the $6P_{3/2}$ or $6P_{1/2}$ state depending on which lasing transition is under consideration, and state 2 is the $6S_{1/2}$ state

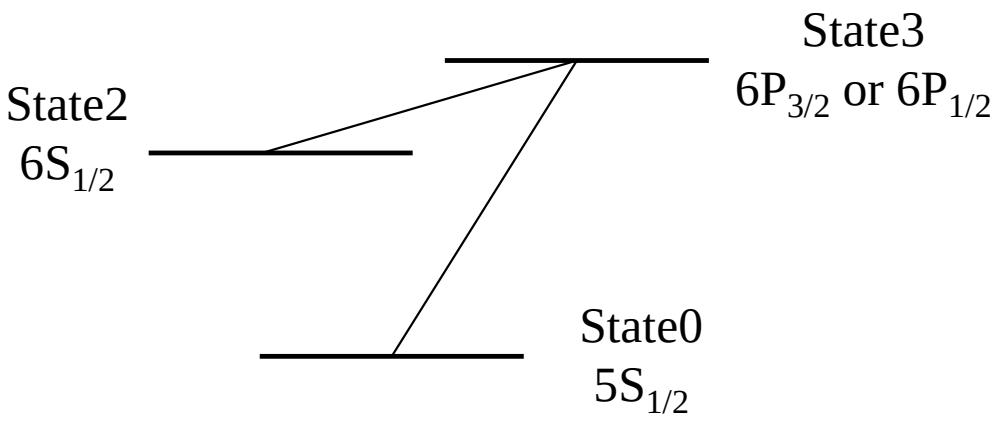

Figure 4.10: Populated states used for both scenarios of model.

In the first scenario lasing action from the $6P_{3/2}$ or $6P_{1/2}$ state to the $6S_{1/2}$ state is considered to proceed very rapidly. At the end of the lasing process the number density of each of the three states is 1/3 the total number density ($n_0=n_2=n_3=1/3n$) for the $6P_{1/2}$-$6S_{1/2}$ transition, and due to degeneracy arguments $n_3=n/2$ and $n_o=n_2=n/4$ for the $6P_{3/2}$-$6S_{1/2}$ transition. Thus, the IR output energy per pulse at 2.79 μm can be found by equation 4.7

$$E = (\frac{1}{3}\mathrm{nV})\mathrm{h}\nu_{32}, \tag{4.7}$$

and at 2.73 by equation 4.8

$$E = (\frac{1}{2}\mathrm{nV})\mathrm{h}\nu_{32}, \tag{4.8}$$

where V is the pump volume and ν_{32} the lasing frequency.

Table 4.3: Calculated IR pulse energy at varying Rb number density for scenario 1 of the above model.

Rb Number Density ($x10^{13}$ cm^{-3})	IR Pulse Energy at 2.73μm (μJ)	IR Pulse Energy at 2.79μm (μJ)
6.5	2.3	1.4
14	4.7	3.1
28	9.5	6.1
52	17.4	11.4

These values are ~3 orders of magnitude larger than the experimental results that will be presented. This perhaps suggests a more realistic scenario occurs when the lasing rate from state 3 to 2 is considered to be much slower than the transitions from state 0 to 3 or state 2 to 0 with gain saturation occurring almost immediately. In this case the lasing intensity is much greater (~10^3) than the saturation intensities given in Table 2.4 (~4 x 10^{-3} W/cm^2). Assuming spontaneous emission along the lasing transitions occurs immediately within the heat pipe entrance and is amplified through the pump volume, the upper asymptotic limit of laser gain applies,

$$I(z) = I_o + \gamma_o I_{\mathrm{sat}} z, \tag{4.9}$$

where input intensity I_o is considered negligible, γ_o is the small signal gain coefficient, I_{sat} is the saturation intensity, and z is the gain path length. With this assumption the IR pulse energy at 2.79 μm is

$$E = \left(\frac{1}{2}\mathrm{nV}\right) \mathrm{h}\nu_{32} A_{32} \tau, \tag{4.10}$$

and at 2.73 μm is

$$E = \left(\frac{2}{3}\mathrm{nV}\right) \mathrm{h}\nu_{32} A_{32} \tau, \tag{4.11}$$

where V is the pump volume, A_{32} is the Einstein A coefficient, and τ is the pulse width (10 ns). Results of equations 4.4 and 4.5 are listed in Table 4.2.

As was shown in the previous sections, the results from scenario 2 differ from those observed by ~2 orders of magnitude. There are, however, several factors not being considered here that can impact the accuracy to the above results appreciably. A first thing to consider is that the IR emission is essentially the fraction of amplified spontaneous emission occurring just inside the heat pipe that forward propagates through the solid angle that overlaps the gain volume. All emission that does not propagate in this direction, therefore, detracts from the available energy the forward propagating emission could have removed through stimulated emission. Another factor is in the γ_o term in equation 4.3. The value used for lineshape was not an integrated value, but that at line center instead, thus omitting a portion of energy that should have been calculated. The

uncertainty in the pump beam's intensity distribution, as well as the true temperature of the alkali vapor can also change the results of the model. In fact, both of these quantities used in the previous analysis are more than likely overvalued.

Table 4.4: Calculated IR pulse energy at varying Rb number density for scenario 2 of the above model.

Rb Number Density ($x10^{13}$ cm^{-3})	IR Pulse Energy at 2.73μm (μJ)	IR Pulse Energy at 2.79μm (μJ)
6.5	0.2	0.1
14	0.3	0.2
28	0.6	0.4
52	1.2	0.7

Sources of Uncertainty

As was mentioned, a large source of error is in defining the effective cross sectional area and energy distribution of the pump laser. The laser burn shown in Figure 4.11 is Figure 3.2 normalized, and it was analyzed with ImageJ software to determine the area to be used for data analysis. The region was shown to have a standard deviation of 5% and area of 7.1 mm^2. This area is used for all calculated experimental results. A suggested topic for future work would be to better characterize this area with a more appropriate tool such as a beam profiler.

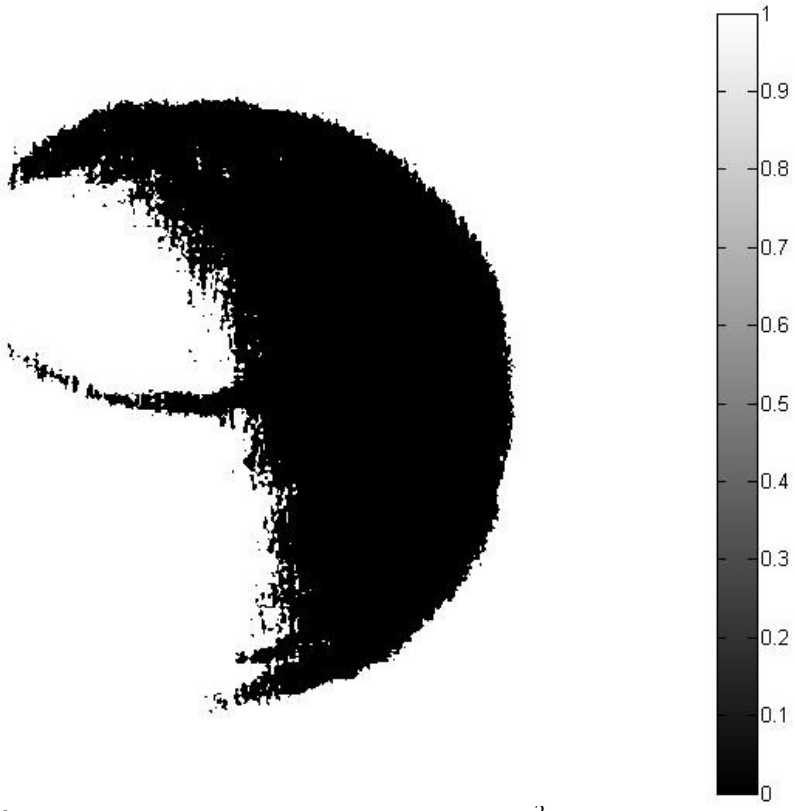

Figure 4.11: Effective area used in data Analysis (7.1mm^2).

Another significant source of uncertainty was in defining the true temperature of the rubidium within the heat pipe. The heater block temperature was measured with a thermocouple and used as the actual temperature of the rubidium within the heat pipe. It is expected, however, the inside walls were as much as 10-20 $^{\circ}$C cooler than the heating block, changing the rubidium vapor pressure significantly.

To quantify the large uncertainties in this work, a very simple argument can be made to bring the results of scenario two in the model to within an order of magnitude of those measured. If, for instance, the temperature of the rubidium is actually 175 $^{\circ}$C while the temperature controllers are reading 190 $^{\circ}$C, rubidium number density is ~50% less

than expected. If cross sectional area is less than the 7.1 mm^2 used in calculations, and if the fact that the spontaneous emission at the beginning of the heat pipe is not utilizing the entire pump volume is taken into consideration, this further reduces the gap between calculated and measured energy. For simplicity, let this account for another factor of 3. Now if the backward propagating light removes half to the energy that could have been consumed by that moving forward, all of these factors contribute to the measured IR signals being ~1/12 of those expected. This simplification still does not take into account all of the energy lost in emission in all other directions, which is also sizable. The construction of a laser cavity, and better diagnostic equipment, therefore, is greatly needed to further understand this system.

V. Conclusions

It has been demonstrated here that mirrorless lasing in Rubidium vapor at 2.73 μm and 2.79 μm is possible with direct optical excitation at 420.2 nm and 421.7 nm respectively. With the pump intensities used, it was shown there exists a very low pump threshold, and bleaching occurs rapidly despite increasing Rb concentration. It is suspected this result is associated with second order effects including multiphoton ionization.

It has been shown that the high intensity pump beam used for optical excitation created significant power broadening in the system. This excitation method was compared to previous work conducted with a continuous wave laser source and showed similar trends in the data.

The individual effects of helium, ethane, and argon buffer gas were also presented. The addition of each gas showed a deleterious effect to IR lasing, fully quenching the signal at less than 50 Torr. The $6P_{1/2}$-$6S_{1/2}$ was quenched at about twice the rate of $6P_{3/2}$-$6S_{1/2}$ although each transition reacted similarly to each gas. Argon proved the least effective at quenching of any the three gases, eliminating signal completely at ~45 Torr for the $6P_{3/2}$-$6S_{1/2}$ transition and ~25 Torr for the of $6P_{1/2}$-$6S_{1/2}$ transition. Ethane and helium showed similar quenching effects, eliminating signal at ~15 Torr for the $6P_{3/2}$-$6S_{1/2}$ transition and ~7 Torr for the of $6P_{1/2}$-$6S_{1/2}$ transition.

A simplified model was presented that predicted energies in the tens to hundreds of nanojoules. It was argued that experimental uncertainties could affect these results significantly enough to bring them down to the energies observed in this work. The two

major uncertainties were in the determination of the temperature of the rubidium and the energy distribution in the pump beam.

In light of this analysis, it does not seem, even if building and optimizing a cavity around this system, that a mid IR laser could be scaled to high enough output powers to serve as an effective infrared countermeasure capable of defeating a heat seeking missile or similar device.

Recommendations for Future Work

In order to further verify the similarities between the data to that of Sharma, increased heat pipe temperatures are necessary to achieve higher rubidium number densities. It could then be seen whether or not IR lasing is completely eliminated as witnessed by Sharma, or if the higher pump intensities and pulsed pump source in this work had some other effect. It could also be seen if IR output continues to asymptote in the bleached limit at higher rubidium concentrations or if the IR signal begins to take on another trend.

Measuring the true intensity distribution of the pump beam with a more suitable diagnostic, as well as obtaining a more trusted value for rubidium temperature could improve modeling efforts.

Filling the gaps between Sharma's continuous wave pump source and the much higher intensity pulsed pump source here could also help elucidate some of the higher order processes and ionization mechanisms that seem to occur at higher rubidium concentrations.

Bibliography

Bearman, Physical Review Letters, "Ionization and Energy Pooling in Laser-Excited Na Vapor", Vol. 41, 1227-1230 (1979)

Borodin, "Associative ionization of excited 5^2P rubidium atoms", Optics and Spectroscopy, Vol. 39, 231 (1975)

Bogachev, A. "Diode-Pumped Caesium Vapour Laser with Closed-Cycle Laser-Active Medium Circulation," Quantum Electronic, Vol.42, No. 2, 95-98 (2012)

Brown, Kirk, "Collisional Dynamics, Lasing and Stimulated Raman Scattering in Optically Pumped Cesium and Potassium Vapors", Air Force Institute of Technology (AU), Wright-Patterson AFB OH, March 2012

Diemer, U. "Infrared Atomic Cs Laser Based On Optical Pumping of Cs_2 Molecules," Chemical Physics Letters Vol.176, No. 1, 135-140 (1991)

Huennekens, J. "Ionization, Excitation of High-Lying Atomic states, and Molecular Fluorescence in Cs Vapor Excited at λ=455.7 and 459.4nm," Physical Review A Vol.31, No. 1, 196-209 (1985)

Klennert, W. "Development of a Compact Heat Pipe Oven for Optically Pumped Alkali Laser Research," Center of Excellence for High Energy Lasers. Kirtland Air Force Base, NM (2012)

Kowalczyk, P., "Asymptotic potentials and coupling terms of excited sodium atoms in thermal collisions", Chemical Physics Letters, Vol. 68, 203 (1973)

Krupke, W. "New Class of CW High-Power Diode-Pumped Alkali Lasers (DPALs)," UCRL-PROC-203398, Lawrence Livermore National Laboratory. April 2006.

Krupke, W. "Resonance Transition 795-nm Rubidium Laser," Optics Letters Vol.28, No. 23, 2336-2338 (2003)

Lucatorto, T., "Efficient Laser Production of a Na^+ Ground-State Plasma Column: Absorption Spectroscopy and Photoionization Measurement of $Na^{+"}$, Physical Review Letters, Vol.37, 428 (1976)

Lucatorto, T. "Laser Excitation and Ionization of Dense Atomic Vapors," Applied Optics Vol.19, No. 23, 3948-3956 (1980)

Page, R. “Diode-Pumped Alkali Atom Lasers Final Report,” Contract W-7405-Eng-48 Project 03-LW-024, Lawrence Livermore National Laboratory. February 2005.

Polak-Dingles, J., “Observation of Structure in Laser-Induced Penning and Associative Ionization in Crossed-Beam Na + Na Collisions”, Physical Review Letters, Vol. 44, 1663 (1980)

Rabinowitz, P. “Continuous Optically Pumped Cs Laser,” Applied Optics Vol.1, No. 4, 513-516 (1962)

Sansonettia, J. “Handbook of Basic Atomic Spectroscopic Data,” National Institute of Standards and Technology, Gaithersburg, Maryland 20899-0001 (2005)

Schawlow, A. “Infrared and Optical Masers,” Physical Review Vol.112, No. 6, 1940-1949 (1958)

Sharma, A. “Continuous-Wave Mirrorless Lasing in Optically Pumped Atomic Cs and Rb Vapors,” Applied Physics B Vol.39, No. 3, 209-211 (1981)

Smith, A.V., Physical Review A, Vol. 22, 577 (1980)

Sorokin, P. “Infrared Lasers Resulting from Giant Pulse Laser Excitation of Alkali Metal Molecules,” J. Chem. Phys Vol.51, No. 7, 2929-2931 (1969)

Sorokin, P. “Infrared Lasers Resulting from Photo dissociation of CS_2 and Rb_2,” J. Chem. Phys Vol.54, No. 5, 2184-2190 (1971)

Steck, Daniel A, “Rubidium 87 D Line Data,” available online at http://steck.us.alkalidata (revision 2.1, 1 September 2008).

Sulham,CA. “Blue and Infrared Stimulated Emission from Alkali Vapors Pumped through Two-Photon Absorption,” Applied Physics Letters Vol.101, No. 1-2, 57-63 (2010)

Titterton, D. “Mid-infrared Semiconductor Optoelectronics,” Springer Series in Optical Sciences Vol.118, 635-691 (2006)

Zhdanov, B. “Highly efficient optically pumped cesium vapor laser,” Optics Communications Vol.260, No. 2, 696-698 (2006)

Zhdanov, B. “Diode-Pumped 10W Continuous Wave Cesium Laser,” Optics Letters Vol.32, No. 15, 2167-2169 (2007)

REPORT DOCUMENTATION PAGE		*Form Approved* *OMB No. 0704–0188*

The public reporting burden for this collection of information is estimated to average 1 hour per response, including the time for reviewing instructions, searching existing data sources, gathering and maintaining the data needed, and completing and reviewing the collection of information. Send comments regarding this burden estimate or any other aspect of this collection of information, including suggestions for reducing this burden to Department of Defense, Washington Headquarters Services, Directorate for Information Operations and Reports (0704–0188), 1215 Jefferson Davis Highway, Suite 1204, Arlington, VA 22202–4302. Respondents should be aware that notwithstanding any other provision of law, no person shall be subject to any penalty for failing to comply with a collection of information if it does not display a currently valid OMB control number. PLEASE DO NOT RETURN YOUR FORM TO THE ABOVE ADDRESS.

1. REPORT DATE (DD–MM–YYYY) 21-03-2013	2. REPORT TYPE Master's Thesis	3. DATES COVERED *(From — To)* September 2012 – March 2013

4. TITLE AND SUBTITLE Mirrorless Lasing in Optically Pumped Rubidium Vapor	5a. CONTRACT NUMBER 5b. GRANT NUMBER 5c. PROGRAM ELEMENT NUMBER
6. AUTHOR(S) Richards, Ryan, M	5d. PROJECT NUMBER 5e. TASK NUMBER 5f. WORK UNIT NUMBER
7. PERFORMING ORGANIZATION NAME(S) AND ADDRESS(ES) Air Force Institute of Technology Graduate School of Engineering and Management (AFIT/ENY) 2950 Hobson Way WPAFB OH 45433-7765	8. PERFORMING ORGANIZATION REPORT NUMBER AFIT-ENP-13-M-41
9. SPONSORING / MONITORING AGENCY NAME(S) AND ADDRESS(ES) Dr. Harro Ackermann Senior Technical Advisor HEL Joint Technology Office 801 University Blvd. SE, Suite 209 Albuquerque, NM 87106 Phone: 505-248-8208 Email: harro.ackermann@jto.hpc.mil	10. SPONSOR/MONITOR'S ACRONYM(S) HELJTO 11. SPONSOR/MONITOR'S REPORT NUMBER(S)

12. DISTRIBUTION / AVAILABILITY STATEMENT
APPROVED FOR PUBLIC RELEASE; DISTRIBUTION UNLIMITED

13. SUPPLEMENTARY NOTES This material is declared a work of the U.S. Government and is not subject to copyright protection in the United States.

14. ABSTRACT

Mirrorless lasing has been successfully demonstrated in a Rubidium heat pipe. Lasing was observed on the $6^2P_{3/2}$-$6^2S_{1/2}$ energy transition at 2.73 μm and on the $6^2P_{1/2}$-$6^2S_{1/2}$ transition at 2.79 μm. The transitions were optically pumped from $5^2S_{1/2}$–$6^2P_{3/2}$ at 420.2 nm and from $5^2S_{1/2}$–$6^2P_{1/2}$ at 421.7 nm, respectively. The $5^2S_{1/2}$–$6^2P_{3/2}$ transition was excited over a 36 GHz band, while the $5^2S_{1/2}$–$6^2P_{1/2}$ transition was excited over a 24 GHz band. Both pump transitions showed a high degree of saturation and only a small fraction (<1%) of the incident pump energy was absorbed. Output energies of up to 5 nJ were obtained at 2.73 μm and of up to 5.4 nJ at 2.79 μm when pumped at pulse energies of ~4 mJ. Both transitions experienced bleaching at this ~4 mJ pump energy, limiting further IR output energy. Increasing rubidium concentration at bleached pump energies showed no increase in laser energy after ~170 °C, likely due to second order processes. Slope efficiency for both transitions, however, increased linearly with rubidium concentration up to 11 x 10^{-6}. The addition of small amounts of argon, helium, and ethane (5-45 Torr) were found to fully quench lasing action on both transitions.

15. SUBJECT TERMS

16. SECURITY CLASSIFICATION OF:			17. LIMITATION OF ABSTRACT	18. NUMBER OF PAGES	19a. NAME OF RESPONSIBLE PERSON Dr. Glen Perram - ENP
a. REPORT U	b. ABSTRACT U	c. THIS PAGE U	UU	55	19b. TELEPHONE NUMBER (Include Area Code) (937)255-3636, ext 4504